Linear augmented Slater-type orbital study of Pt–5*d*-transition-metal alloying

R. E. Watson, J. W. Davenport, and M. Weinert
Physics Department, Brookhaven National Laboratory, Upton, New York 11973-5000
(Received 29 May 1987)

We have used a self-consistent density-functional theory with an augmented Slater-type-orbital basis to calculate the heats of formation, charge components, and densities of states for ordered 5*d*-transition-metal–platinum alloys. Crystal structures considered were CsCl, CuAu-I, AuCd, CrB, Cu_3Au, Al_3Ti, $MoSi_2$, and $MoPt_2$, though not all structures were calculated for each alloy system. Calculated heats of formation are in accord with the limited experimental data for close-packed systems; however, the ill-packed CrB structure cannot be described sufficiently well with our muffin-tin potentials. Correct phase-diagram behavior, i.e., the correct structure at a given composition and the competition between phases at different composition, is predicted. Charge transfer was inspected with use of the orbital population and Wigner-Seitz sphere counts as were two observables sensitive to charge behavior. These were the electron contact density at the nucleus and the initial-state shift of core-electron energy levels. Neither of these are simply related to the charge-transfer terms. In addition, the charge transfer does not correlate with traditional notions concerning differences in electronegativity. One complication, encountered previously in calculations for Au alloys, is that a significant component of the change in charge at an atomic site upon alloying has nothing to do with charge transfer, hybridization, or screening in the traditional chemical sense but is, instead, simply associated with the overlap of tails of charge best understood as being associated with orbitals centered on neighboring sites. Thus while it has been long recognized that orbital population analyses are not unique because they are strongly affected by the details of how overlap is dealt with, it turns out that analyses of charge transfer, based on integrating charge over a Wigner-Seitz cell or sphere, are also blurred by the overlapping.

I. INTRODUCTION

Platinum, with its almost filled 5*d* bands, is on the one hand chemically active—witness its catalytic properties—while on the other hand it is the most noble-metal-like of the transition elements. When alloyed with elements to the left-hand end of the transition-metal row, Pt tends to have its 5*d* bands filled. For example, the bonding of but one La atom with five Pt atoms does this in $LaPt_5$ and, as a result,[1] there is a low density of states at the Fermi level and the compound is diamagnetic. It is apparent that the 5*d* bands are chemically active, with the band-filling tendency an essential feature. In order to advance our understanding of this phenomenon, electronic-structure calculations are reported here from which are inferred the energetics and the charge transfer associated with forming ordered compounds of Pt with its 5*d* transition-metal neighbors, Lu through Ir.

The present investigations employ the linear augmented Slater-type-orbital method[2,3] (LASTO), within the local-density approximation. A summary of our method is given in the Appendix. The calculations are scalar relativistic, that is, spin-orbit coupling has been omitted from the conduction bands, though the core levels are treated fully relativistically. In addition, muffin-tin potentials, which involve spherical potentials within the atomic spheres, have been used. The utilization of muffin-tin, instead of full, crystal potentials represents a substantial economy in computing, but at a cost in rigor. As has already been seen in calculations[4] for Au alloys, LASTO calculations employing muffin-tin potentials yield accurate heats of formation for compounds which are well packed or close-packed, that is fcc-, hcp-, or bcc-like. A heat of formation involves the difference in total energies between that of the compound and those of the elemental metals, and reasonable heats are obtained for well-packed compounds since the elemental metals are *also* close packed. Ill-packed compounds, where a larger fraction of the crystal volume is in the interstitial region and where atomic sites tend to be of lower symmetry, are another matter. Most of the compounds, which are relevant to Pt alloying and will be of concern here, are close packed. The CrB structure, in which PtHf forms, is, however, ill packed and its heat of formation will be seen to be substantially underestimated when muffin-tin potentials are employed.

The plan of the paper is as follows. First, heats of formation, based on total-energy calculations, will be reported and then charge transfer as measured by population analyses, by simply integrating the charge at an atomic site and by observable quantities such as changes in contact densities or in core energy levels, will be considered. The computations will not be described in detail as this has been done elsewhere.[2–5] They involve, for example, special sets of **k** points and the crystal total energy converges rapidly with the size of the **k** basis set as has been shown for the elemental 5*d* transition metals[5] as well as for some of their compounds.[3] Nonoverlapping atomic spheres are used in the calculations for

the compounds and total energies, obtained for the elemental metals with the *same* sphere radii, are used in calculating the heats of formation. Some results for the Pt-Ta system have also been reported[6] previously. These involved crystal structures formed by the stacking of monatomic layers, the purpose being to make contact with the formation of metal adlayers on single-crystal metal substrates and with the formation of multilayer materials. The results suggested that, at least for Pt-Ta, the stacking of close-packed bcc [110] layers is locally stable while globally unstable with respect to the stacking on non-close-packed layers.

Heats of formation will be reported for those ordered Pt 5*d* element crystal structures having unit cells which are small enough to be within our computational means. As a rule, the results are consistent with known phase behavior, i.e., the correct phase, among the competing phases, is predicted at some given composition and competing phases of differing composition are predicted to coexist (or to not coexist) in a phase diagram when that, in fact, is the case. The one notable exception to this success occurs for the calculations of HfPt in the ill-packed CrB structure (similar failures could be expected for other ill-packed structures having unit cells too large for us to deal with here). The heats of formation (per constituent atom) of Pt, and for that matter of Pd and Ni, when alloyed with elements at the left-hand end of the transition-element row are unusual. Most alloy systems display maximum heats of formation at, or near 50%-50% concentrations: Such a concentration lets there be the maximum number of pairs of *unlike atom neighbors* and this enhances the binding. In contrast, the alloys of concern here have their maximum heats skewed well off of 50%-50% concentrations. From simple band-filling arguments one might expect that such a case could arise at a concentration where the composite 5*d* bands are half-filled, implying that the "bonding" electron levels are filled and the "antibonding" empty. If this were so, the Pt-poor alloys would have the larger heats of formation. The reverse is the case and this is manifested in alloy volumes as well as in the heats (i.e., deviations from Vegard's law are more marked[7] for the Ni-, Pd-, and Pt-rich, than they are in the Ni-, Pd-, and Pt-poor, alloys). This skewing is more pronounced for the alloys of Ni, Pd, or Pt than it is for the alloys of their neighbors, the noble metals and Co, Rh, and Ir. The skewing would appear to be associated with the filling of the bands having strong Ni, Pd, or Pt *d* character with the possibility, then, of moving these levels away from the Fermi level. This contrasts with the alloys of other transition metals where the Fermi level is pinned somewhere within their *d* bands.

Charge transfer in the Pt alloys is very similar to that of the Au alloys with the most marked difference being that while the Au atoms lose some of their *d* count upon alloying, Pt sustains a near-zero change in its 5*d* count. In other words a depletion, due to hybridization of another wave-function character into the occupied Pt-like 5*d* bands, accompanies the above-mentioned band filling. Energetically, this is necessary because the Coulomb energy cost of filling the 5*d* bands alone would be prohibitive. What is surprising is how completely these two tendencies cancel one another out. Another feature, common to these as well as to the gold alloys, is the presence of substantial "overlap" contributions in the charge transfer. These are manifested as high-*l* components in the charge density which can best be understood as being the tails of *s*, *p*, or *d* wave function character which is centered on neighboring atom sites.

II. HEATS OF FORMATION

The calculated heats of formation for the 50%-50% binary alloys are plotted in Fig. 1. Different phases of the same compound are calculated with the same molecular volume, and this volume is derived from observed crystallographic data for the alloy composition in question or, lacking this, on the observed deviations from Vegard's law for other compositions. The observed phase behavior[8] for the 50%-50% compounds is tabulated at the bottom of Fig. 1. Compared with many other alloy systems, knowledge of the Pt alloy phase behavior is incomplete and there are apparent inconsistencies which may have arisen from the observation of metastable phases. PtTa, for example, is two phase at low temperatures, but it is generally accepted that there is a high-temperature phase whose structure is unknown though its x-ray pattern is reported to be fcc-like. It is, of course, the low-temperature behavior with which the present calculated heats should be compared. Heats of

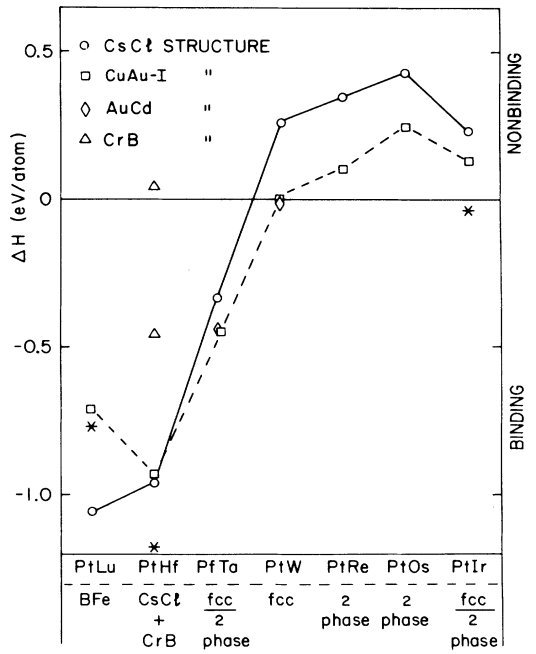

FIG. 1. Calculated heats of formation of 50%-50% Pt–5*d*-element ordered-binary-alloy phases. The asterisks are experimentally obtained heats (enthalpies) and the panel at the bottom indicates the observed phase diagram behavior at this concentration. (The horizontal bars for PtTa and PtIr separate differing high- and low-temperature phase behavior.)

almost one-half of an electron volt per atom are calculated for the ordered PtTa phases but, as will be seen, these are suppressed by competition from phases at other compositions and the band-theory results, like experiment, indicate PtTa to be two phase. Essentially zero-valued heats are calculated for PtW; however, here a disordered fcc phase, which being disordered we are not prepared to deal with, prevails. The Pt-Ir system is an fcc solid solution at high temperatures, but a miscibility gap occurs at low temperatures so that it as well as Pt-Re and Pt-Os are to be considered two phase at 50%-50%. The positive heats calculated at this concentration for the ordered compounds are consistent with this (the experimental ΔH, plotted for PtIr, is reported for a temperature where the system is immiscible). Turning to the left-hand end of the row where the larger heats occur, PtLu forms in the BFe structure which has a larger unit cell than we can deal with. Of the CsCl and CuAu-I structures for which calculations have been done, one would expect the CsCl to be the most stable, as it is calculated to be, since it is the stable phase for PdLu and PtSc and since no 50%-50% compounds are formed from the Ni and Sc columns of the Periodic Table having the CuAu-I structure. PtHf forms in the CrB and, at slightly off 50%-50% concentrations, in the CsCl structures. There are serious problems with the calculated heat for the CrB structure of which more will be said shortly. We see that the CsCl-structure ΔH is again lower than that for the CuAu-I structures as it should be. While the CsCl structure should be more strongly bound than CuAu-I for PtLu and PtHf, inspection of the phase behavior of other transition-metal alloy systems suggests that the CuAu-I or the AuCd (which involves a different stacking of close-packed layers[9]) would likely be the more-stable phase for PtTa and PtW if stable phases, in fact, occurred at 50%-50%. The present calculations show the two structures, AuCd and CuAu-I, to be essentially degenerate for these systems.

There are experimental heats of formation data for PtLu and PtHf which are indicated in the figure.[10] They differ by several tenths of an eV/atom from the lowest-lying calculated CsCl-structure points. This can be deemed to represent agreement between theory and experiment since the scatter in experimental values, when more than one experimental determination has been made for some system, is of this order for such strongly bonded systems.

The one failure in Fig. 1 is associated with PtHf in the CrB structure. This structure is displayed in Fig. 2, where it is seen to consist of Pt-Hf pairs arranged parallel to the y axis with rather considerable gaps between pairs along that axis. The $\times$'s in the figure indicate the midpoints of these gaps for the $z=\frac{1}{4}$ plane of atoms. The structure is ill packed in two senses. First, placing nonoverlapping atomic spheres around the atomic sites leads to a substantially larger fraction of the crystal volume lying in the interstitial region than is the case for the close-packed structures. Second, the atomic sites and their associated crystal potentials are of low symmetry involving nonspherical terms with l as low as 1. Calculations for this crystal structure are complicated by

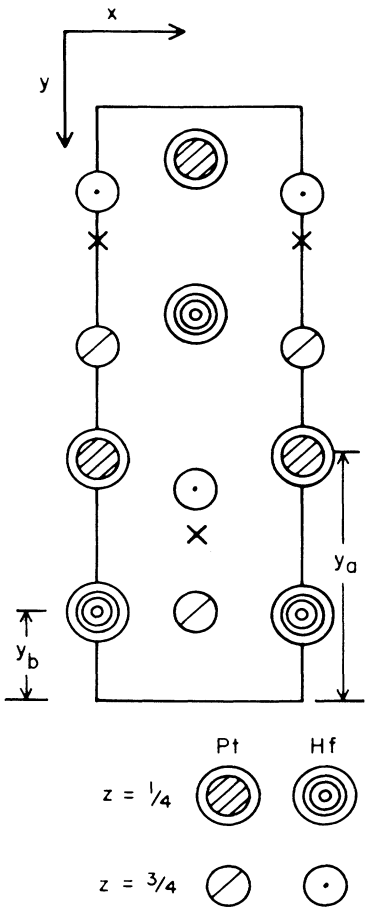

FIG. 2. The CrB structure, in which PtHf forms, as viewed along the crystal's Z axis. Note that the atoms lie in two planes at Z equal to $\frac{1}{4}$ and $\frac{3}{4}$. See text for the meaning of the $\times$'s.

the fact that there are two coordinates, y_a and y_b, which define where atoms lie within the unit cell. The total energy of the system is sensitive to these coordinates, which in the case of PtHf were not determined crystallographically and hence must be obtained variationally in the course of the calculations. A calculation employing a muffin-tin potential yielded the ΔH of $+0.05$ eV/atom, which is ~ 1 eV/atom less bound than the value obtained for the better-packed CsCl structure with which it should be degenerate. In other words, the total energy for the CrB structure was ~ 1 eV/atom *worse* than the energies for either the CsCl, CuAu-I, and AuCd structures *or for the elemental metals* in their close-packed structures (the latter being employed to obtain heats of formation). A second calculation was done where empty spheres were added at the midpoints of the gaps, i.e., at the $\times$'s in the figure plus the equivalent points in the $z=\frac{3}{4}$ plane. This resulted in a ΔH of -0.45 eV/atom, halving the extent to which the energy of this structure is out of line relative to the others (it did not matter much as to whether the solutions in the empty spheres are limited to $l=0$ terms or whether

higher l's were taken as well). It should be noted that the introduction of these empty spheres still leaves the system with a larger than normal fraction of its space in the interstitial region. It would appear that full potential calculations, which are substantially more expensive than those employed here, are necessary in any serious attempt to correctly place an ill-packed structure, such as CrB, relative to the well-packed systems.

Calculated heats of formation for the Pt-rich 3:1 compounds, taken to be in the Cu_3Au and Al_3Ti structures, are shown in Fig. 3. These two structures are related in a simple way: Cubic Cu_3Au can be visualized as an fcc lattice with Au's at the cube corners and Cu's on the faces, which implies that every other (100) plane is composed of one-half Cu and one-half Au. Granted this, tetragonal Al_3Ti is obtained by interchanging the Cu's and Au's in every other Cu-Au plane, followed by a tetragonal distortion normal to these planes. Of the three systems displaying ordered phases,[6] Pt_3Lu, Pt_3Hf, and Pt_3Ta, the relative stability of the Cu_3Au versus the Al_3Ti structure is correctly predicted. In the case of Pt_3Ta, the Al_3Ti structure is observed slightly off exact stoichiometry (the Cu_3Ti and Pt_3Nb structures were beyond our computational means). In the cases of Pt_3W and Pt_3Re, disordered fcc structures prevail over the ordered compounds while Pt_3Os, and, at low temperatures, Pt_3Ir are two phase. The nonbinding heats obtained for these last two are consistent with this.

Two experimental values for the heat of formation of Pt_3Hf are displayed in Fig. 3, one of which is in accord

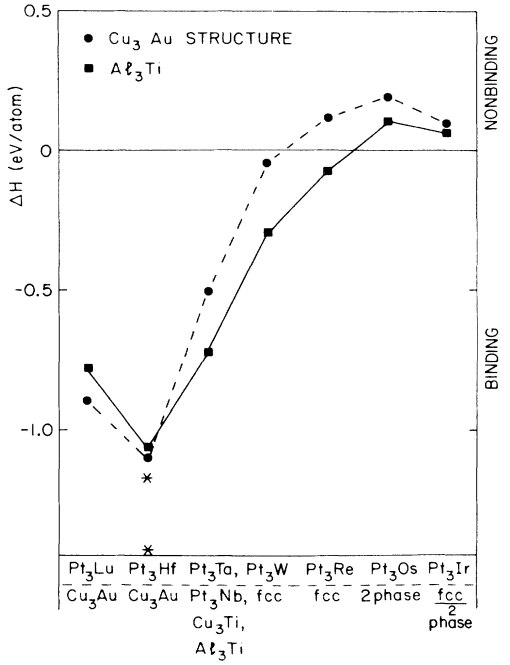

FIG. 3. Calculated heats of formation for Pt_3X (X being a $5d$ element) compounds. The asterisks are experimentally obtained heats and the panel at the bottom indicates the observed phase diagram behavior at this concentration. (The horizontal bar for Pt_3Ir indicates differing phase behavior at high and low temperatures.)

with the calculations. Overall, the calculated quantities of Fig. 3 are consistent with known phase diagram and thermodynamic data.

The calculated heats are plotted as a function of alloy concentration for Pt-Hf, Pt-Ta, and Pt-W in Fig. 4. Consider Pt-Hf first: The fact that the CsCl structure heat lies below the dashed line drawn between the zero by Hf and the Cu_3Au-structure heat implies that the CsCl structure is stable relative to a two-phase mix consisting of pure Hf and Pt_3Hf in the Cu_3Au structure. The fact that the Cu_3Au-structure heat lies below the line drawn between the CsCl-structure ΔH and the zero for pure Pt implies that the Cu_3Au-structure phase is similarly stable relative to the CsCl phase plus pure Pt. Calculations were also done for Pt_2Hf in the $MoSi_2$ structure, which is reported to exist off stoichiometry at a $Pt_{0.6}Hf_{0.4}$ composition. The fact that the ΔH for stoichiometric Pt_2Hf lies above the line drawn between the CsCl and Cu_3Au structures indicates that, according to these local-density-theory calculations, the stoichiometric $MoSi_2$ phase is unstable relative to a mix of the two phases.

The PtTa and Pt_2Ta calculations have been reported previously,[6] where the issue of concern was the relative stability of stacking close-packed nonatomic layers (as often obtained by epitaxial growth) versus the stacking of less-close-packed layers (as frequently occurs in crystal structures, such as the $MoSi_2$). Here we see the 50%-50% compounds suppressed by the Al_3Ti-structure phase in combination with pure Ta. This suppression would be more severe if we had similar heats for the Ta-rich σ and $A15$ phases which occur, and we then considered the suppression between these and the Al_3Ti phase. The $MoPt_2$ structure heat almost lies below the Al_3Ti-structure pure Ta line, this structure being the fcc-like analog of bcc-like $MoSi_2$—the two being related by an orthorhombic distortion. Actually, Pt_2Ta forms in its own distorted version of the $MoPt_2$ structure with lower site symmetry. The cross on the figure is our estimate of ΔH for the Pt_2Ta-structure phase: The calculation was done for a restricted set of **k** points and the vertical bar is our estimate of the uncertainties associated with this. Being of lower symmetry, the phase has been penalized by our use of muffin-tin potentials and is

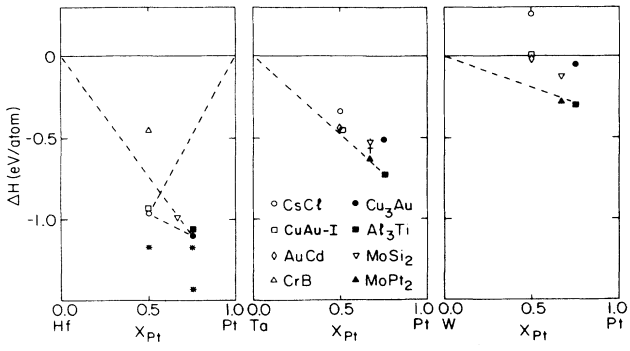

FIG. 4. Calculated heats of formation for various phases of Pt-Hf, Pt-Ta, and Pt-W as a function of alloy composition. The asterisks are experimentally observed heats.

calculated to be slightly less stable than the $MoPt_2$-structure phase. In the process, it just misses being calculated to be stable.

The only ordered phase which is generally accepted as occurring in the Pt-W system is Pt_2W in the $MoPt_2$ structure. This is calculated to be moderately stable relative to the Al_3Ti structure plus pure W. Actually, a disordered fcc, rather than the ordered Al_3Ti, is observed at the Pt_3W composition. The fact that the $MoPt_2$ structure is calculated to be only moderately stable suggests that the ordered Al_3Ti-structure phase is almost degenerate with the disordered fcc phase and that, if any sublattice ordering were to be observed for Pt_3W, it would be of this type.

Overall, the set of calculated heats is in agreement with what is known experimentally. The ΔH for PtHf, when taken in the low-site-symmetry CrB structure, is in serious error, and that for the Pt_2Ta is in modest error, relative to the heats calculated for the well-packed compounds.

III. CHARGE TRANSFER

A. Population counts

Charge transfer may be measured by integrating the valence charge within Wigner-Seitz (WS) cells or spheres. One complication associated with doing this is the choice of what fraction of the molecular unit cell is to be associated with each of the atomic species in the compound. As will be seen, there is yet another complication. An alternative measure, granted the Slater-type-orbital (STO) basis, is to make molecular-orbital population analyses[3] of the valence charge *centered* on a site, though extending into neighboring sites. As has been recognized for a long time, this is complicated by the problem of the nonorthogonality of orbitals centered on different sites, and there is no completely satisfactory way of apportioning the overlap charge. We have employed the Mulliken[11] and the modified Mulliken[3] schemes for handling the nonorthogonality.

The three measures of the total charge transfer on or off the Pt site are plotted for the CsCl, CuAu-I, Cu_3Au, and Al_3Ti structures in Fig. 5. The sign convention of the figure is that plus indicates valence charge transfer onto the Pt site and minus off. The Mulliken and modified Mulliken charge transfers do not vary smoothly with alloy constituent, and this is largely associated with overlaps due to the *p*-like Slater-type orbitals, which are the most diffuse of the STO's.

There is the distinct suggestion that an alloy system in the CsCl structure undergoes more charge transfer than it does when in the CuAu-I. The same tendency was seen previously[4] in the Au alloys. While it is difficult to quantify, the Pt site transfer is less in the Pt_3X alloys, than in the 50%-50% compounds, when the alloying involves right-hand elements such as W, Re, Os, and Ir. This is to be expected since Pt is the majority element in the former set of alloys. However, this is *not* the case for the Pt-Lu and Pt-Hf systems, the two systems where particularly strong alloy formation occurs. For these systems, the charge transfer at the majority, Pt, site in

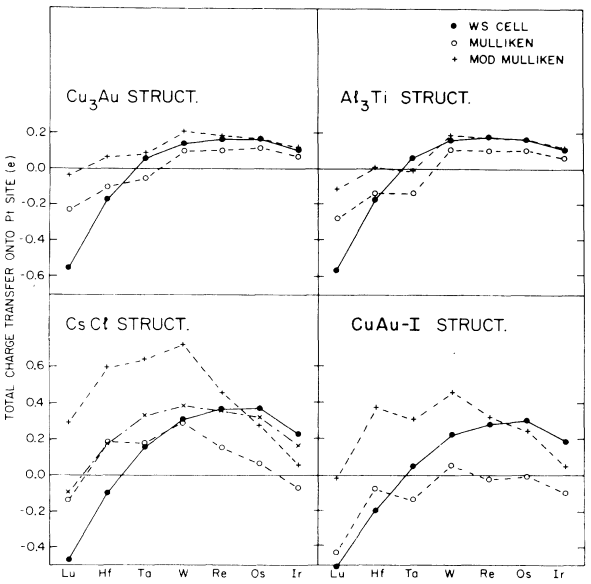

FIG. 5. Calculated charge transfer on or off the Pt site (positive for electron transfer onto Pt) for various Pt 5*d* element compounds as measured by Wigner-Seitz sphere integrations and by Mulliken and modified Mulliken population analyses. See text for a discussion of the dot-dashed curve plotted for the CsCl structure.

the 3:1 compounds is every bit as large as that in the 50%-50% compounds. Remember that the heats of formation per atom are also greater in these 3:1 compounds.

The most striking feature of Fig. 5 is that the calculated charge transfer is not consistent with notions concerning electronegativity trends. Conventional wisdom would have Lu being the most electropositive of the elements considered here, followed by Hf and, in turn Ta. If so, the largest transfer *onto* Pt should occur when it's alloyed with Lu (followed by Hf and Ta), and here the reverse occurs with the strong suggestion that Pt actually loses charge to Lu.

Individual *s*, *p*, and *d* charge transfer terms at both the Pt and the other sites are plotted in Fig. 6. The Al_3Ti structure is not represented since its results are almost identical to those of the Cu_3Au structure. Both the WS-cell samplings and the Mulliken population changes are shown, and while they do not always agree in numerical detail, they display common trends. Perhaps the most notable feature is that, except for Pt-Lu, the Pt site *d* transfer is essentially zero valued despite the fact that in all these alloys the bands which are discernibly Pt *d*-like are filled by the alloying process. This band filling of $\sim\frac{1}{2}$ an electron per Pt is accompanied by a depletion of *d* count due to hybridization of other wave-function character into the already occupied Pt *d* bands, and it would appear that these two factors succeed in almost perfectly canceling one another out. Δn_d was similarly constant at the Au site in the previously reported results[4] for Au alloyed with the 5*d* elements; however, in

that case Au "lost" about one-tenth of a d-electron charge rather than the essentially zero-valued depletion seen here.

The variation in charge transfer with a differing alloy component is concentrated, largely, in the Δn_p of the Pt and the Δn_p plus Δn_d of the other sites. From simple d-band–d-band bonding arguments, one would expect the other sites, with their greater number of d holes than Pt, to gain in d count by hybridization of those d holes into the occupied Pt d bands. However, this only occurs for Ir, which is adjacent to Pt in the Periodic Table, and for Lu whose bands are so nearly empty that the hybridization of its hole states into the occupied Pt bands dominates, causing the increase in d-like (and p-like) Lu character. As might be expected, the trends seen in Fig. 6 bear a distinct resemblance to those obtained previous-

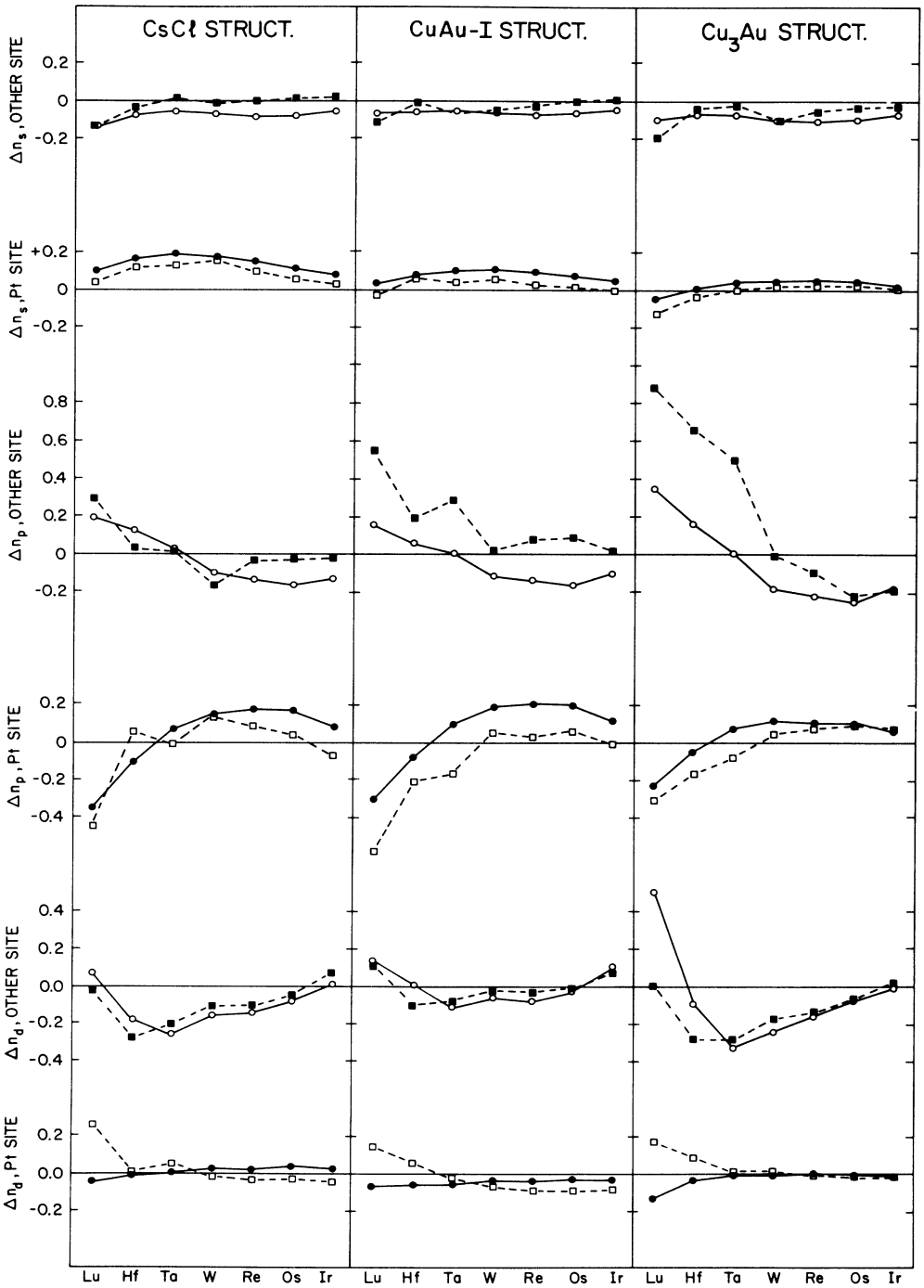

FIG. 6. Individual calculated s, p, and d charge-transfer components calculated for Pt $5d$ element compounds in the CsCl, CuAu-I, and Cu_3Au structures. Mulliken populations (dashed lines) and Winger-Seitz–sphere integrations (solid lines) are shown.

ly[4] for the Au alloys.

Our basis set contains l values up to eight inside the spheres [see Eq. (A3)]. As a result the spherically averaged charge density also contains components up to $l=8$. While these are incorporated as tails in the orbitals of the orbital population analyses, they are not included in the s, p, and d Wigner-Seitz cell terms of Fig. 6. For the present calculations, the partial charges for $3<l<8$, are plotted in Fig. 7 for the alloys in the CsCl structure. Similar charge terms appear[12] in the elemental metals. These high-l components are a real feature of the charge density and they are best viewed as associated with the tails of s-, p-, and d-band orbitals centered on other sites. Now, in the CsCl structure the eight nearest neighbors are unlike neighbors. What if these contribute a tail charge in the compound similar to what they sampled from each other in the elemental metal? Different atoms with their differing volumes will sample the tail charge to a different extent. Let us then assume that the sampling scales as the volumes in the elemental metals, i.e.,

$$\rho_B(l\geq 3)=(V_B/V_A)\rho_A(l\geq 3)\ , \tag{1}$$

where ρ_B is the B-site sampling in the AB compound and ρ_A is the value[12] in elemental metal A. The dashed curves of Fig. 7 are the result of employing Eq. (1). The agreement at both the Pt and the other sites is remarkable, granted the crudity of the assumptions implicit in Eq. (1). Similar plots for the other crystal structures work out much more poorly. These structures have like as well as unlike atoms in the nearest-neighbor shell introducing the complexity of apportioning like and unlike atom tail charge at some given site.

The consequences of the high-l components to the charge transfer are to be seen in the CsCl-structure segment of Fig. 5 and in Fig. 8. In the former case, attributing the $l\geq 3$ charge components to the eight closest neighbors of the CsCl structure, which are unlike, one can define

$$\rho_B=\rho_B(l<3)+\rho_A(l\geq 3) \tag{2}$$

as the charge centered on a B site in these 50%-50% compounds. Doing this yields the dot-dashed curve of the CsCl-structure segment of Fig. 5. The curve is in better register with the orbital population shifts than is the WS-cell sampling. The contributions of these high-l components to the change in Wigner-Seitz cell charge are plotted in Fig. 8. They represent a substantial fraction of the total charge transfer which occurs.

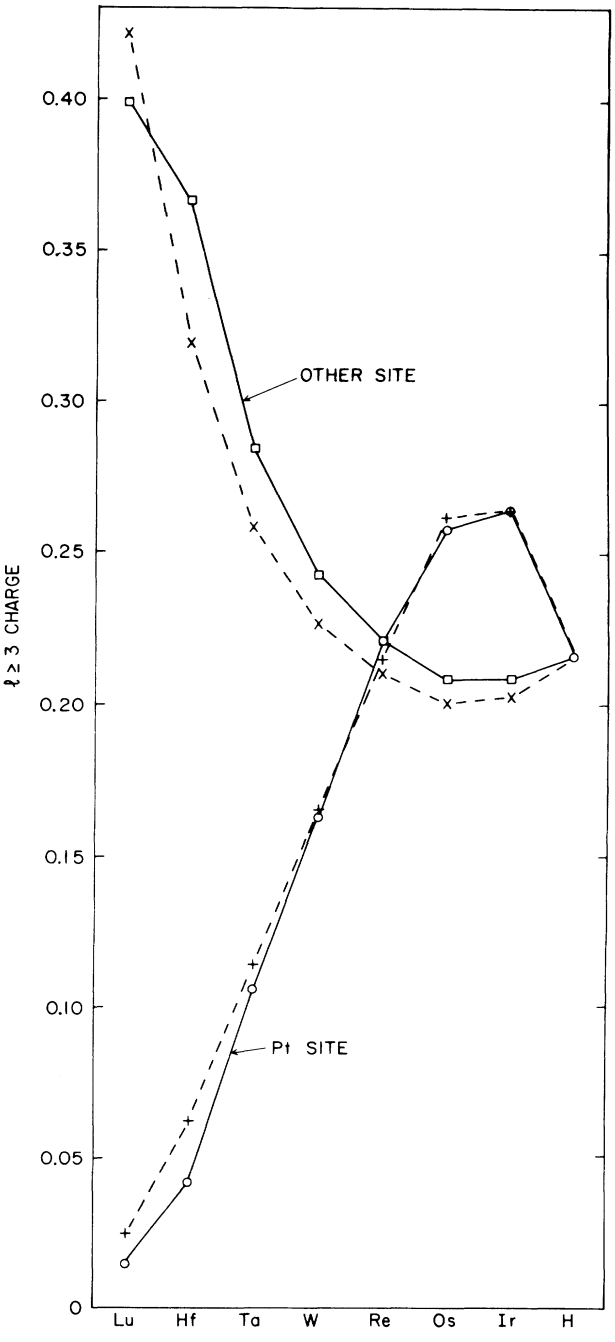

FIG. 7. The $l>2$ charge components within the Pt's and the other 5d elements Wigner-Seitz spheres as obtained for the CsCl structure compounds. The dashed curves are based on scaling the $l>2$ components, obtained for the elemental metals, with Eq. (1).

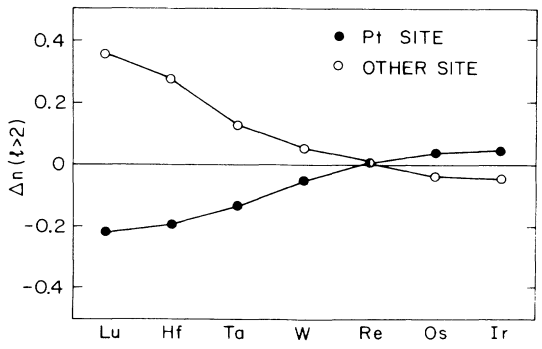

FIG. 8. The charge transfer associated with $l>2$ angular momentum charge components residing in the Wigner-Seitz spheres as calculated for Pt 5d element compounds in the CsCl structure relative to the elemental metals.

B. Contact densities

One experimental measure of charge transfer is the electron charge density at the nucleus (contact density) $\rho(0)$, as is sampled by the Mössbauer isomer shift. Pt and a number of the other $5d$ elements have nuclei with nuclear transitions suitable for such experiments. The density at the nucleus involves s-like electron character (with small relativistic $p_{1/2}$ contributions as well). The change in contact density upon alloying, $\Delta\rho(0)$, may arise either from the change in s-like valence electron count at the site, Δn_s, or to changes in the core and valence electron charge already there. These changes are due to relaxation in response to overall changes in valence charge. On some occasions,[4,13] both this screening and the Δn_s terms appear to contribute substantially to $\Delta\rho(0)$ while, on other occasions,[14] it would appear that there is little apparent screening and the Δn_s terms predominate. If comparison is to be made between contact density changes for different elements, it becomes necessary to somehow normalize $\Delta\rho(0)$ for effects associated with changing nuclear charge. At the top of Fig. 9, $\Delta\rho(0)$, which is the difference between the contact density due to the valence electrons in the elemental metal, $\rho(0)$, and that in the CsCl-structure alloy, is normalized by dividing the elemental metal's $\rho(0)$ [which was calculated with an augmented plane-wave (APW) sphere radius equal to that used in the compounds]. Now, the elemental metal valence s electron count is roughly three-quarters of an electron across the $5d$ row so one might further normalize the upper figure by multiplying $\Delta\rho(0)/\rho(0)$ by $\frac{4}{3}$ as is done with the right-hand scale on the figure. Then the $\Delta\rho(0)$ are normalized with respect to the contact density of an s-electron having the average s-like character of the elemental metal's conduction bands. For all the alloys there is an increase in contact density at the Pt site and losses at the other sites. This is consistent with the view that Pt is the most electronegative of these metals though, of course, there is no reason to apply electronegativity arguments to s transfer alone. Insight can be obtained by further dividing the shifts, normalized with the $\frac{4}{3}$ factor, by, say, the Wigner-Seitz sphere samplings of Δn_s, the change in valence–s-electron count, i.e.,

$$R_\rho \equiv \frac{4}{3}\frac{\Delta\rho(0)}{\Delta n_s \rho(0)} \ . \tag{3}$$

This is done in the bottom section of Fig. 9. A ratio of $+1$ corresponds to a $\Delta\rho(0)$ which is consistent with the transfer of s-electron charge which has the character of the average s-like charge appropriate to the elemental metal. Ratios which do not equal $+1$ are due either to deviations in the transferred charge from the elemental character or because of the s-charge screening in response to overall valence electron transfer [note: the screening due to an increase (or decrease) of valence charge will cause an expansion (or contraction) of the s-like charge already on the site causing a decrease (or increase) in its contact density]. The variation in R_ρ, and the deviations from values of $+1$, are such as to suggest that screening is playing an active role. This is even more clearly the case for the $\Delta\rho(0)$ calculated for Pt-rich alloys in the Cu_3Au structure. These are plotted in Fig. 10. The Pt site $\Delta\rho(0)/\rho(0)$ ratios are a factor of 2 to 3 smaller than is the case for the CsCl structure, and this

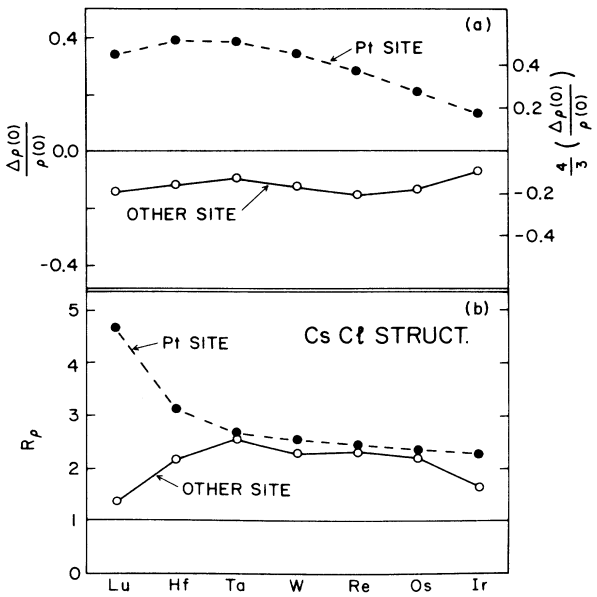

FIG. 9. Normalized changes in the conduction-electron contributions to the contact density at the nucleus associated with going from the elemental metals to the Pt $5d$ element compounds in the CsCl structure. (a) $\Delta\rho(0)/\rho(0)$ and (b) R_ρ as defined in Eq. (3).

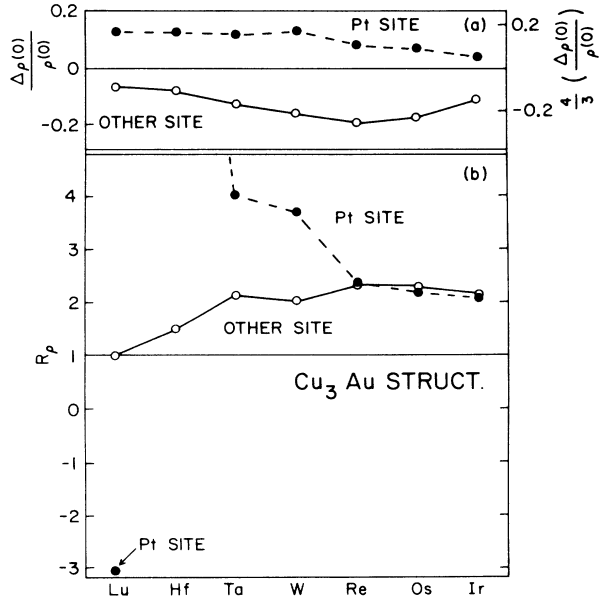

FIG. 10. Normalized changes in the conduction-electron contribution to the contact density at the nucleus associated with going from the elemental metals to the Pt-rich–$5d$-element compounds in the Cu_3Au structure. (a) $\Delta\rho(0)/\rho(0)$ and (b) R_ρ as defined in Eq. (3).

is not surprising since the majority of nearest neighbors to a Pt site are now Pt's. In contrast, the other atomic species has only Pt's as nearest neighbors in both structures and the $\Delta\rho(0)/\rho(0)$ are much the same. Dividing these ratios by Δn_s yields R_ρ, which are similar for the other sites in the two structures; however, the Pt R_ρ values go off scale for Pt_3Hf and reverse sign for Pt_3La. This strongly suggests that screening effects are dominating.

C. Core-level shifts

Another traditional measure of charge transfer is the energy-level shift of a core electron as sampled by photoemission. Both initial-state effects, associated with the change in chemical environment and final-state effects, associated with the change in screening of the hole left behind by the photoelectron, contribute to the measured level shift. The binding energy is the energy required to promote an electron from the core level to the Fermi level. We have previously defined[15] the initial-state part as the binding energy obtained with frozen orbitals. Then the final-state part is the difference between the frozen part and the actual (self-consistent) binding energy. We have also shown that the shift in the initial-state part is approximately given by the shift in the one-electron eigenvalue. In this paper we will look at the change in eigenvalue of the $4f$ levels since these are readily seen experimentally and suffer the least lifetime broadening. The level shift is then $\Delta(\varepsilon_{4f}-\varepsilon_F)$ where $\varepsilon_{4f}-\varepsilon_F$ of the compound is measured with respect to the elemental metal. Calculated $\Delta(\varepsilon_{4f}-\varepsilon_F)$ are plotted for the $4f_{5/2}$ core levels in Fig. 11. Greater binding, that is negative $\Delta(\varepsilon_{4f}-\varepsilon_F)$, would seem to imply deeper potentials, hence charge transfer off a site. However, as a rule, core-level shifts of the same sign occur at both the Pt and the other site, and this is inconsistent with $\Delta(\varepsilon_{4f}-\varepsilon_F)$ reflecting overall charge transfer. Consider now the level shifts at the other sites: These correlate

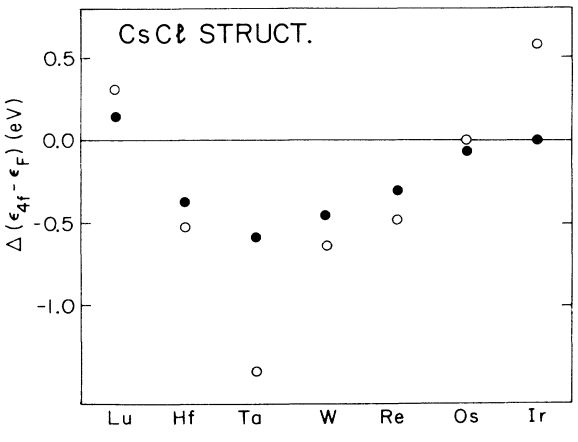

FIG. 11. The initial-state chemical shift $(\varepsilon_{4f}-\varepsilon_F)$ for the $4f_{5/2}$ core levels associated with going from the elemental metals to the compounds in the CsCl structure. Solid circles denote the Pt site shifts while the open circles indicate the shifts at the other sites.

with the sites Δn_d and Δn_p (see Fig. 6). If these shifts are attributed to d electron transfer (since the d charge is more compact and hence has a stronger Coulomb interaction with the core electron) an estimate can be made of the effective d-core electron interaction

$$U_{d\text{-}c} \equiv \frac{\Delta(\varepsilon_{4f}-\varepsilon_F)}{\Delta n_d} \tag{4}$$

having values of the order of 2–3 eV. (Values of $U_{d\text{-}c}$ closer to 5 eV can be derived from the previous[4] results for Au alloys and for the other sites in the Pt_3X compounds here.) Problems arise when considering the Pt sites. The Δn_d are near-zero valued while the Δn_p and Δn_s anticorrelate with the level shifts, that is they indicate charge transfer onto the Pt sites at the same time as the shifts indicate greater binding. Thus, the $U_{d\text{-}c}$ are negative as defined in Eq. (4). It would, therefore, appear that shifting Fermi levels are playing a dominating role in the Pt site $\Delta(\varepsilon_{4f}-\varepsilon_F)$, thus masking any chemically induced core-level shifts. The reason for this will be suggested in the next section. Even though the $\Delta(\varepsilon_{4f}-\varepsilon_F)$ seem to reflect the Δn_d at the other sites here and at both Au and other sites in the Au compounds,[4] the Pt results suggest that these correlations may not be altogether meaningful. Core-level photoemission experiments have sometimes been thought a poor source of chemical information because of changes in final-state screening. One might hope to estimate these screening effects and correct experimental values for them. But here we have a case where the initial-state shifts have no transparent relationship to the site chemistry.

IV. ELECTRON DENSITIES OF STATES

Densities of states $N(\varepsilon)$ represent a more traditional measure of valence electron populations than do the measures considered in the preceding section. $N(\varepsilon)$ appear in Fig. 12 for PtLu, PtHf, PtTa, and PtIr in the CsCl structure. The first three of these represent systems where there are substantial heats of formation in the ordered 50%-50% compounds, while the last involves Pt alloyed to its immediate $5d$ neighbor. The first column indicates the total density of states while the second and third, with a change in vertical scale, indicate the partial densities of states at the Pt and other sites, respectively. The attributions as to site occupation are based on integrations of the electron charge over the atomic spheres (not the site Wigner-Seitz spheres), hence the site $N(\varepsilon)$ add up to somewhat less than the total $N(\varepsilon)$. The most striking feature of the PtLu, PtHf, and PtTa $N(\varepsilon)$ is the tall peak below the Fermi level which is primarily Pt-like in nature, as indicated by the partial densities of states, though with some wave-function character of the other site hybridized into these levels. The width of this feature of $N(\varepsilon)$ narrows on going from the Ta to the Hf and, in turn, to the Lu compound. This is associated with an increased separation between Pt atoms in the lattice. Using an elegantly simple derivation, Heine concluded[16] that the d-band width should vary as R^{-5}, R being the atomic separation, and subsequent investigation,[17] where the bandwidths were

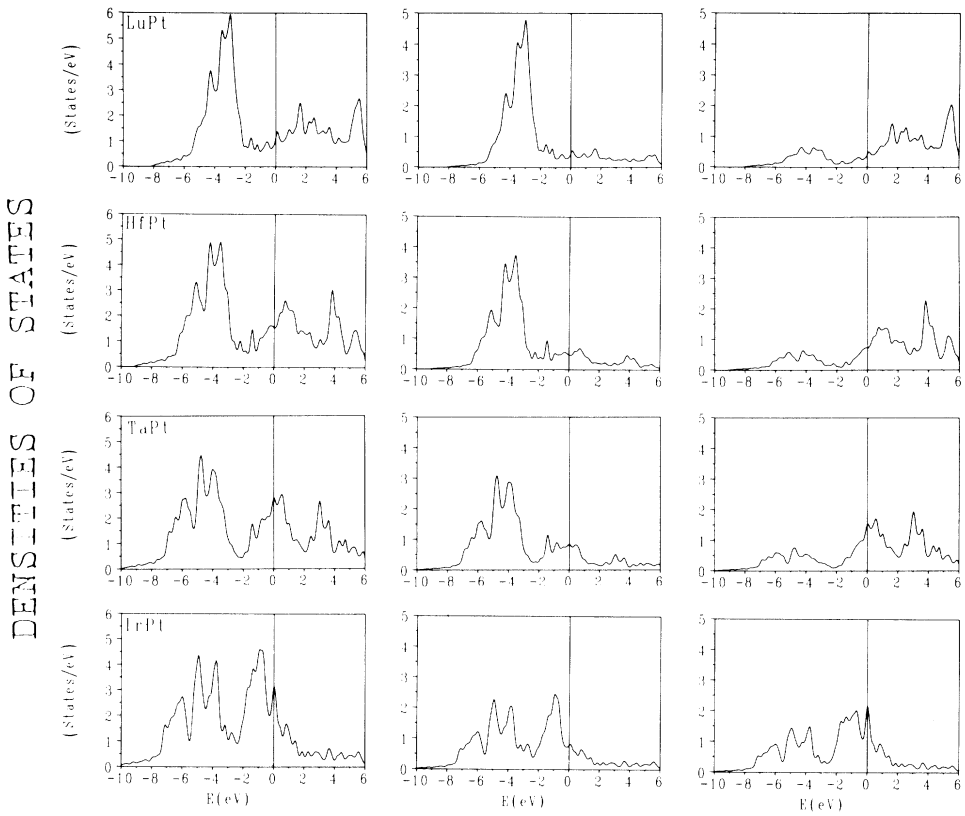

FIG. 12. Calculated densities of states for PtLu, PtHf, PtTa, and PtIr in the CsCl structure. The left-hand column is the full density of states $N(\varepsilon)$, while the middle and right-hand columns are the individual site partial densities of states associated with the Pt and other sites, respectively. The apportioning of $N(\varepsilon)$ to these separate sites was based on integrating electron charge densities over APW spheres. Note the change in vertical scale on going from the full to the partial densities of states. The Fermi level is at the zero of energy.

explicitly evaluated as a function of R, indicates somewhat smaller exponents, say, ~ 4.5. The variation in the Pt-like feature, below the Fermi level, has a width which scales very closely as $R^{-4.5}$. Here R is the Pt-Pt separation. The bands which are primarily associated with Lu, Hf, and Ta sites straddle the Fermi level as they must in order to have the necessary valence electron occupancy. Their partial densities of states are lower in height and broader than the Pt features as should be the case, i.e., at some given R, their bandwidths are markedly greater than Pt's because their d orbitals are markedly more diffuse.

In the case of PtIr one has heavily overlapping bands where Ir wave-function character has almost as much weight, $\sim\frac{3}{4}$th's, of Pt in the deep-lying bands. Similarly, there is substantial Pt character in the upper part of the bands though it is significantly absent from the $N(\varepsilon)$ spike right at the Fermi level. The lower-lying features of the PtIr $N(\varepsilon)$ resemble those of the compounds above and its width scales pretty well as $R^{-4.5}$ off the like features in the other band structures. The extent to which PtIr, with its heavily overlapping and hybridized bands, has an $N(\varepsilon)$ which falls naturally in a sequence with those of the other three compounds, is remarkable.

In the sequence PtLu, PtHf, and PtTa, the Fermi level must fall increasingly higher in the bands in order to accommodate the increasing number of occupied electron levels, and this causes the strong, low-lying, features of $N(\varepsilon)$ to lie increasingly far below the Fermi level. The shift in the center of gravity of these Pt-like features, relative to ε_F, is[18] $\sim 1\frac{1}{2}$ eV on going from PtLu to PtTa. These features are primarily Pt $5d$-like in character. Now core-level positions do not precisely trace such features since a core electron does not suffer band hybridization (which causes shifts in level positions) and it samples the crystal potential differently. Experience from photoemission[19] suggests that for metals such as Pt and Au the core levels have shifts of the same sign but smaller in magnitude than the d levels. This is occurring here: Inspection of Fig. 11 shows a Pt site shift in $(\varepsilon_{4f}-\varepsilon_F)$ of $\sim\frac{3}{4}$ eV on going from PtLu to PtTa. It would, indeed, seem that the initial-state Pt core-level shifts, at least those on the left-hand side of Fig. 11, are controlled by what is best viewed as a shift in Fermi level rather than by "chemical" changes in the potential as sampled by the core.

The density of states for Pt_3Ta in the Cu_3Au structure is represented in Fig. 13. "Separated bands" are seen

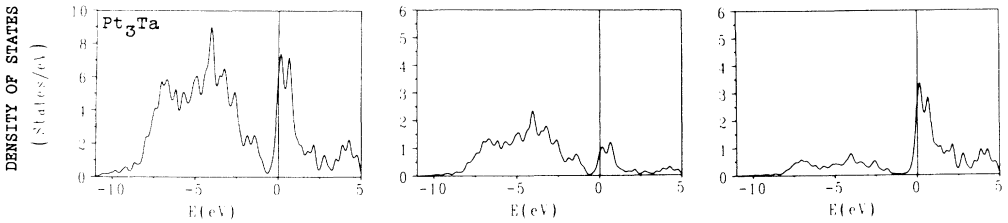

FIG. 13. Calculated densities of states, as in Fig. 12, obtained here for Pt_3Ta in the Cu_3Au structure.

much as was the case for PtTa in Fig. 12: i.e., the high density of states below ε_F is primarily Pt-like while that at and above ε_F is mostly Ta-like. Now the Pt-like features are broad in energy while those of Ta are narrow. This is understandable in terms of the changes in Ta-Ta and Pt-Pt distances in the two structures where the Pt in Pt_3Ta, being the concentrated species, are closer together while the dilute Ta are farther apart. Ignoring a packing consideration beyond the nearest-like-neighbor distance, and scaling as $R^{-4.5}$, we have for the Pt site

$$\left[\frac{R(Cu_3Au)}{R(CsCl)}\right]^{-4.5}=1.85$$

so a CsCl-structure subband width of 4 eV scales to 7.4 eV in the Cu_3Au structure; and for the Ta site

$$\left[\frac{R(Cu_3Au)}{R(CsCl)}\right]^{-4.5}=0.39$$

so a CsCl-structure subband width of 5.5 eV scales to 2.1 eV in the Cu_3Au structure. There is some arbitrariness in reading off the subband widths from the $N(\varepsilon)$ plots, but there is semiquantitative agreement with this oversimplified scaling of the $N(\varepsilon)$ behavior.

The most striking population changes, seen in Fig. 6, are associated with the p-electron populations. The p densities of states, appropriate to the compounds represented in Fig. 12, are plotted in Fig. 14. Consider, again, the sequence PtLu, PtHf, and PtTa and note the greatly magnified vertical scale as compared with Fig. 12. In the region below the Fermi level the overall amplitude of the p character at the Pt site decreases, while that at the other sites increases, on going from PtTa to PtLu. All the site's terms appear to increase along the same sequence at energies above ε_F. The changing p character in either the region above or below ε_F appears to occur across the band energies and not involve states at some well-defined energy alone. If one takes a ruler to the plot, one discovers that the p $N(\varepsilon)$ peaks fall at different energies below ε_F, e.g., for PtLu the most-pronounced Pt site peaks occur between -2 and 3 eV and -4 to $4\frac{1}{2}$ eV, while the Lu peaks occur at -5 and between -3 and -4 eV. All these peaks may be found in the full $N(\varepsilon)$ of Fig. 12. At and above ε_F, the p electron $N(\varepsilon)$ peaks of the two sites fall at the same energies. It would seem then, that p hybridization of the two sites largely involves quite different states in the Pt-like region of the band structure but occurs with common states in the other site's region.

As noted above the amount of p hybridization of one site's character into the bands "belonging" to the other site increases on going from PtTa to PtLu. In this sense, then, PtLu involves more chemically active bonding than PtHf or, in turn, PtTa, and this is consistent with chemical intuition even if not supported by overall charge-transfer tendencies. Note that this p hybridization apparently involves the transfer of electrons off electronegative Pt and onto electropositive Lu. The other region of marked variation in the charge-transfer terms of Fig. 6 occurs for the Lu-Hf-Ta site Δn_d where there is a sign reversal on going from PtaTa where Ta loses d charge to PtLu where Lu gains such charge. This appears to be a saturation effect, namely by the time one gets to Lu, the metal has so few occupied d states to hybridize into the empty bands of Pt, and so many empty levels to mix into the occupied Pt states, that Lu's d count can only increase.

V. DISCUSSION

In summary, we have performed first-principles, self-consistent, density-functional calculations on a series of platinum–5d-transition-metal alloys. These calculations which involve no adjustable parameters are of roughly equal quality as those[20] of Williams, Gelatt, and Moruzzi in the 4d row. Both could be improved by adding non-muffin-tin terms to the potential. In addition, in contrast to Williams *et al.* our calculations include relativistic effects other than spin-orbit splittings. The work reported in this paper has concentrated on total-energy calculations and estimates of wave-function character. It was observed that accurate heats of formation were obtained for ordered Pt compounds, provided that those compounds were as well packed as the elemental metals whose total energies were used as references. On the whole, the relative heats of formation of one compound versus another were correctly predicted for compounds of the same composition and different structure and for compounds of differing composition. Granted this, this offers the prospect of *a priori* estimates of phase diagrams and the relative stabilities of metastable systems. This success was seen to break down when ill-packed systems, such as the CrB structure illustrated in Fig. 2, were considered. This appears to be due to the fact that muffin-tin potentials were employed in the calculations and their shortcomings become more severe in poorly

packed systems of low site symmetry. Presumably, these problems are removed by going to full potentials with their nonspherical terms inside the atomic spheres and the nonconstant behavior in the interstitial region. It is nevertheless of interest to know how well muffin-tin potentials work since they are both simpler and more economic to apply. The present results suggest that there is a large arena where they suffice. The issue of applying full potentials to lower-symmetry crystals will be the subject of future work.

The trend in the heats of formation, shown in Fig. 1, is very similar to what we found previously for gold alloys.[4] This trend has also been found in the density-functional calculations in the 4*d* row[20] as well as in phenomenological calculations such as Miedema's,[21] Pettifor's,[22] and Watson and Bennett's.[23] Basically, it results because bonding is maximized when the *d* band is roughly half full. This occurs when the average *d* electron number (9 for Pt, 8 for Ir, etc.) is near 5. For PtLu, $\bar{n}=(n_{\mathrm{Pt}}+n_{\mathrm{Lu}})/2$ is 5.5, and so it should produce the largest heat. Compared with the 4*d* row, the 5*d*-row bonding is stronger presumably as a result of larger bandwidths.

As in the gold alloys,[4] we find that while the phenom-

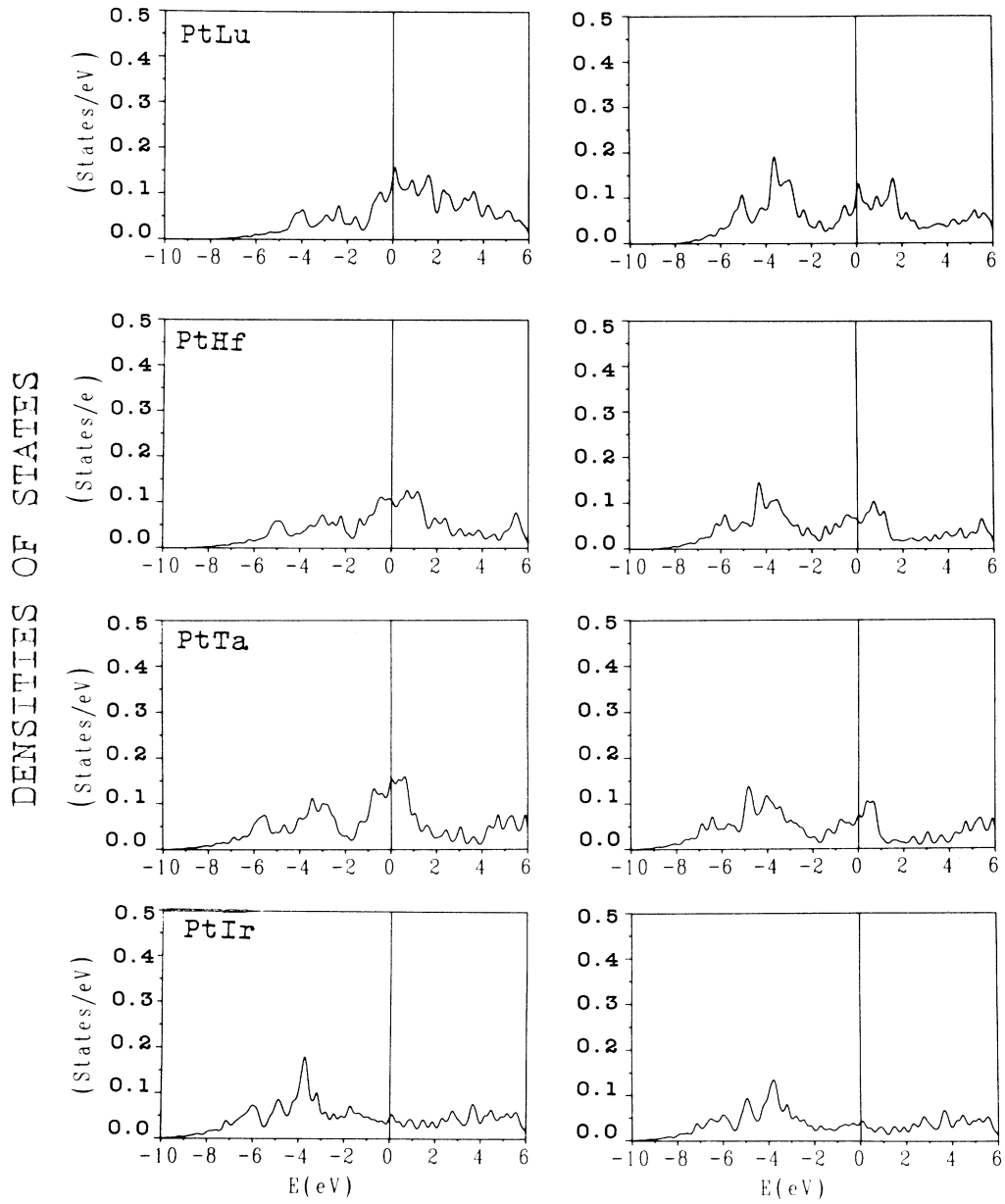

FIG. 14. The *p*-like charge components of the individual site densities of states as calculated for PtLu, PtHf, PtTa, and PtIr in the CsCl structure. The left-hand column is the Pt site density of states, and the right-hand column is that of the other site. The *p* components of the charge were inferred from APW-sphere integrations. Note: The Fermi level is at the zero of energy as in Fig. 12; however, the vertical scales are greatly magnified over those in Fig. 12.

enological models can reproduce the heats they fail to describe the wave-function character. The most interesting cases here are Pt-Lu, Pt-Hf, and Pt-Ta. These systems are the only strongly bound ones in the Pt $5d$ sequence and their bonding and wave-function character vary measurably from system to system. It was seen that charge transfer does not resemble traditional ideas concerning electronegativity trends. Also, the two experimental measures of valence electron behavior considered, namely contact charge densities at the nucleus and core-electron-energy level shifts, do not clearly reflect bonding differences. The contact densities, which may be sampled by Mössbauer isomer shifts, are a measure of the electron density at the nucleus. However, screening due to changing valence electron behavior appears to be as important as the change in count of those valence electrons having a contact density for the alloys of concern here. This masks any simple interpretation of such contact density changes. The initial-state effects, concerning the position of a core-electron energy level measured with respect to the Fermi level, were considered (final-state screening which further complicates matters was neglected). It was observed that the Pt site level shifts were primarily due to shifts best attributed to the Fermi level and *not* to chemical shifts of core-level positions. Thus, even without the complication of final-state screening, the level shifts do not readily indicate chemical effects.

One of the observations made here and previously[4] for Au alloys, is the presence of high-l components in the charge density at a site—a situation not admitted in most band-theory publications discussing wave-function character. These high-l components are readily understood as arising from the tails of s-, p-, and d-like orbitals centered on neighboring atom sites (see the discussion concerning Figs. 7 and 8). These "overlap" terms can represent a significant fraction of the charge transferred on or off a site and they have nothing to do with charge transfer, hybridization, or screening effects in the normal sense of the word. One vexing complication is that part of the s-, p-, and d-like charge changes at a site must also arise from such overlap instead of from bonding. From experience with the high-l components where over one-half the overlap charge is f-like (and over one-half the remainder g-like) one expects the s, p, and d overlap terms to be substantial. It is difficult to disentangle overlap contribution from other terms though one might hope to make a start by comparing orbital population analyses, such as the Mulliken scheme (which presume orbitals centered on sites and extending into neighboring sites), with the Wigner-Seitz cell integration of the charge which analyzes charge in terms of l components in a single site. Despite scatter, the orbital populations lie below the WS counts for the s and p (and right-hand end of the d) character at the Pt sites with the reverse occurring at the other sites. If

$$\Delta n_l(\text{overlap}) \equiv \Delta n_l(\text{WS}) - \Delta n_l(\text{Mulliken}) \tag{5}$$

is taken to be the measure of overlap contributions, then there are positive Δn_s(overlap) and Δn_p(overlap) terms at Pt sites and negative ones at the other sites. This is *opposite in sign* to the high-l component terms for PtLu through PtRe (and in agreement for PtOs and PtIr) as can be seen by inspection of Fig. 8. The only place of substantive agreement in sign between Eq. (5) and Fig. 8 occurs for the d terms in both sites in PtLu and PtHf, that is, the Δn_d(WS) lie above the Δn_d(Mulliken) at the Lu and Hf sites while lying below at the Pt sites. The sign reversals are surprising, though not out of the question granted that we are dealing with charge differences taken between the elemental metals and the compounds. More-detailed consideration of this issue is perhaps best done using full-potential band calculations where the full complexity of the problem is admitted at the onset. This is a subject for future investigation.

ACKNOWLEDGMENTS

This work was supported by the Division of Materials Sciences, U.S. Department of Energy, under Contract No. DE-AC02-76CH00016 and by a grant of computer time at the National Magnetic Fusion Energy Computing Center, Livermore, California.

APPENDIX

The details of our calculation method have been given elsewhere,[2-5] but we indicate here briefly some technical details. The LASTO method may be viewed as similar to the linear augmented-plane-wave method[24] except that the space between nonoverlapping spheres is spanned by a Bloch sum of Slater-type orbitals instead of plane waves. That is, in the interstitial our basis function is

$$\psi_{inlm}(\mathbf{r}) = \frac{1}{(N_c)^{1/2}} \sum_{\mathbf{R}} \exp(i\mathbf{k}\cdot\mathbf{R}) \phi_{nlm}(\mathbf{r}-\mathbf{R}-\mathbf{t}_i) , \tag{A1}$$

where $\mathbf{R}$ labels a unit cell, $\mathbf{t}_i$ the position of atom i within the unit cell, and ϕ_{nlm} is a Slater-type orbital

$$\phi_{nlm}(\mathbf{r}) = A_n r^{n-1} \exp(-\zeta r) Y_{lm}(\hat{\mathbf{r}}) , \tag{A2}$$

and A_n is the normalization.

In the calculations reported here we used a single $5d$, $6s$, and $6p$ function leading to a 9×9 secular matrix. The ζ's were chosen by minimizing the total energy of the metallic elements and are listed for convenience in Table I.

The Bloch sum (A1) is matched smoothly onto scalar relativistic solutions of the Dirac equation at the sphere boundaries so that inside the spheres

$$\psi_{inlm}(\mathbf{r}) = \sum_{\lambda,u} [\beta_{inlm,\lambda\mu} g_\lambda(r) + \alpha_{inlm,\lambda\mu} \dot{g}_\lambda(r)] Y_{\lambda\mu}(\hat{\mathbf{r}}) , \tag{A3}$$

where $\dot{g}$ is the energy derivative of g exactly as in other linear methods. The sum in (A3) was extended to $\lambda \leq 8$.

The density-functional equations are solved self-consistently using a muffin-tin potential (no overlapping of spheres) and the Hedin-Lundqvist form of the exchange correlation potential. The Coulomb potential was calculated using the pseudocharge density method as detailed by Weinert.[25]

The charge density was constructed by sampling

TABLE I. ζ values used in the calculations [see Eq. (A2)].

	Lu	Hf	Ta	W	Re	Os	Ir	Pt	Au
ζ_{5d}	1.80	2.05	2.19	2.40	2.45	2.53	2.54	2.58	2.50
ζ_{6s}	1.97	2.09	2.18	2.29	2.41	2.51	2.57	2.64	2.70
ζ_{6p}	1.33	1.48	1.61	1.70	1.75	1.80	1.86	1.93	2.00

~ 120 special points in the Brillouin zone for the CsCl and CuAu-I structures and fewer (to maintain the same density of points) in the more complex structures. There are many more points than are needed if the primary purpose of the calculations is to yield total energies; for this 20–30 k points would suffice. The larger number is desirable when constructing density-of-states plots. The eigenvalues near the Fermi level were broadened with the square of a hyperbolic secant (whose integral gives the Fermi distribution) with a temperature of 0.001 atomic units ≈ 300 K. Each eigenvalue was broadened with a Gaussian with a full width at half maximum of 0.25 eV when constructing the densities of states

Finally, we note that, in practice, the reciprocal-space version of Eq. (A1) was used,

$$\psi_{inlm}(\mathbf{r})=\frac{1}{(N_c)^{1/2}}\sum_{\mathbf{G}}\exp[i(\mathbf{k}+\mathbf{G})\cdot(\mathbf{R}-\mathbf{t}_i)] \times\frac{1}{\Omega}\tilde{\phi}_{nlm}(\mathbf{k}+\mathbf{G}) , \tag{A4}$$

where $\mathbf{G}$ is a reciprocal-lattice vector and $\tilde{\phi}$ the Fourier transform of the Slater-type orbital (which is known analytically). Reciprocal-lattice vectors $|\mathbf{G}|<G_{\text{cut}}$ were included in the sum. G_{cut} was typically $3.4\times(2\pi/a)$ for the CsCl structure leading to approximately 180 reciprocal-lattice vectors. This is comparable to the number of G's used in an LAPW calculation (which then requires diagonalization of a 180×180 matrix). Compared to self-consistent LAPW results on the same (muffin-tin) potentials, LASTO energies for the metallic elements are ~ 0.3 eV higher (less binding). This should be regarded as a basis-set error. For the heat of formation this error cancels out and, as shown previously,[3,4] the heats calculated by the two methods agree.

Given the LASTO basis the eigenvalue problem becomes

$$\sum_{N'}H_{NN'}C_{N'}=\varepsilon\sum_{N'}S_{NN'}C_{N'} , \tag{A5}$$

where N is a composite index giving $inlm$. Then the Mulliken population[11] was obtained in the usual way as

$$Q_N=\sum_{N'}\mathrm{Re}\{C_N^*S_{NN'}C_{N'}\} . \tag{A6}$$

The modified Mulliken population is defined in Ref. 3. The Wigner-Seitz population was obtained by smoothly extending the density inside the atomic spheres out to the Wigner-Seitz radius and integrating. (The Wigner-Seitz radius is defined by the volume of the metallic element.) This technique does not guarantee that the sum of the Wigner-Seitz charges is equal to the total number of valence electrons, but it is approximately.

[1]See, e.g., I. D. Weisman, L. H. Bennett, A. J. McAlister, and R. E. Watson, Phys. Rev. B **11**, 82 (1975).

[2]J. W. Davenport, Phys. Rev. B **29**, 2896 (1984).

[3]R. E. Watson, J. W. Davenport, and M. Weinert, Phys. Rev. B **34**, 8421 (1986).

[4]R. E. Watson, J. W. Davenport, and M. Weinert, Phys. Rev. B **35**, 508 (1987).

[5]J. W. Davenport, M. Weinert, and R. E. Watson, Phys. Rev. B **32**, 4876 (1985); J. W. Davenport, R. E. Watson, and M. Weinert, *ibid.* **32**, 4883 (1985).

[6]R. E. Watson, J. W. Davenport, and M. Weinert, Phys. Rev. B **35**, 9284 (1987).

[7]See, e.g., R. E. Watson and L. H. Bennett, Acta Metall. **30**, 1941 (1982).

[8]See, e.g., W. G. Moffatt, *Handbook of Binary Phase Diagrams* (Plenum, Schenectady, New York); phase diagram behavior may also be inferred from tabulations of crystallographic data such as P. Villars and L. D. Calvert, *Pearson's Handbook of Crystallographic Data for Intermetallic Phases* (American Society for Metals, Metals Park, Ohio, 1985).

[9]See, e.g., W. B. Pearson, *The Crystal Chemistry and Physics of Metals and Alloys* (Wiley-Interscience, New York, 1972).

[10]A. recent tabulation of experimental heats may be found in C. Colinet, A. Pasturel, and P. Hicter, CALPHAD: Comput. Coupling Phase Diagrams Thermochem. **9**, 71 (1985).

[11]R. S. Mulliken, J. Chem. Phys. **23**, 1833 (1955).

[12]See Fig. 7 of Ref. 4.

[13]See, e.g., R. E. Watson, L. J. Swartzendruber, and L. H. Bennett, Phys. Rev. B **24**, 6211 (1981).

[14]H. Akai, S. Blügel, R. Zeller, and P. H. Dederichs, Phys. Rev. Lett. **56**, 2407 (1986).

[15]M. Weinert, J. W. Davenport, and R. E. Watson, Phys. Rev. B **34**, 2971 (1986).

[16]V. Heine, Phys. Rev. **153**, 673 (1967).

[17]Unpublished renormalized-atom calculations for several elemental transition metals, as a function of crystal volume, yielded exponents which generally fell between -4 and -5. A value of -4.5 appears to be a reasonable "typical" value.

[18]The position of ε_F, relative to the low-lying Pt-like features of $N(\varepsilon)$, depends both on the band filling and on the spacing of those low-lying features relative to the features near ε_F which are primarily associated with the other site. There is some suggestion that this spacing is slightly smaller in PtTa then in PtLu. If this were not the case, the ε_F shift would be somewhat greater than $1\frac{1}{2}$ eV.

[19]E.g., this can be inferred by comparing Fig. 2 and Table III in T. K. Sham, M. L. Perlman, and R. E. Watson, Phys. Rev. B **19**, 539 (1979).

[20]A. R. Williams, C. D. Gelatt, Jr., and V. L. Moruzzi, Phys. Rev. Lett. **44**, 429 (1980).
[21]A. R. Miedema, P. F. De Chatel, and F. R. De Boer, Physica **100B**, 1 (1980).
[22]D. G. Pettifor, Phys. Rev. Lett. **42**, 846 (1979); Solid State Commun. **28**, 621 (1978).
[23]R. E. Watson and L. H. Bennett, Phys. Rev. Lett. **43**, 1130 (1979); CALPHAD: Comput. Coupling Phase Diagrams Thermochem. **8**, 307 (1984).
[24]See, for example, L. F. Mattheiss and D. R. Hamann, Phys. Rev. B **33**, 823 (1986).
[25]M. Weinert, J. Math. Phys. **22**, 2433 (1981).